Boron-doped diamond electrode: synthesis, characterization, functionalization and analytical applications

Luong, John H. T.; Male, Keith B.; Glennon, Jeremy D.

Publisher's version / Version de l'éditeur:
https://doi.org/10.1039/b910206j
Analyst, 134, 10, pp. 1965-1979, 2009-08-07

Boron-doped diamond electrode: synthesis, characterization, functionalization and analytical applications

John H. T. Luong,*[ab] Keith B. Male[b] and Jeremy D. Glennon[a]

First published as an Advance Article on the web 7th August 2009
DOI: 10.1039/b910206j

In recent years, conductive diamond electrodes for electrochemical applications have been a major focus of research and development. The impetus behind such endeavors could be attributed to their wide potential window, low background current, chemical inertness, and mechanical durability. Several analytes can be oxidized by conducting diamond compared to other carbon-based materials before the breakdown of water in aqueous electrolytes. This is important for detecting and/or identifying species in solution since oxygen and hydrogen evolution do not interfere with the analysis. Thus, conductive diamond electrodes take electrochemical detection into new areas and extend their usefulness to analytes which are not feasible with conventional electrode materials. Different types of diamond electrodes, polycrystalline, microcrystalline, nanocrystalline and ultrananocrystalline, have been synthesized and characterized. Of particular interest is the synthesis of boron-doped diamond (BDD) films by chemical vapor deposition on various substrates. In the tetrahedral diamond lattice, each carbon atom is covalently bonded to its neighbors forming an extremely robust crystalline structure. Some carbon atoms in the lattice are substituted with boron to provide electrical conductivity. Modification strategies of doped diamond electrodes with metallic nanoparticles and/or electropolymerized films are of importance to impart novel characteristics or to improve the performance of diamond electrodes. Biofunctionalization of diamond films is also feasible to foster several useful bioanalytical applications. A plethora of opportunities for nanoscale analytical devices based on conducting diamond is anticipated in the very near future

Introduction

Owing to complete C-sp^3 hybridization and tetrahedral bonding (Fig. 1), diamond displays many unique properties such as chemical inertness, extreme hardness and thermal conductivity, low friction coefficient, and high charge carrier mobilities (Table 1).[1] Natural diamond with extremely high inherent electrical resistivity, with a bandgap of 5.47 eV at $T = 300$ K, cannot be used as an electrode material. However, if p-doped with boron, boron-doped diamond (BDD) will become conductive. Boron doping introduces 'midgap' states to enhance conductivity and electron-transfer reactivity, ~360 meV above the valence band.[2] Boron concentrations (10^{18}–10^{21} atom cm^{-3}) produce a film resistance of 10^4 and 10^{-2} Ω, respectively. Corrosion-resistant and dimensionally stable diamond films can also be

[a]*Analytical and Biological Research Facility (ABCRF), Department of Chemistry, University College Cork (UCC), Ireland. E-mail: j.luong@ucc.ie*
[b]*Biotechnology Research Institute, National Research Council Canada Montreal, Quebec, Canada H4P2R2. E-mail: john.luong@cnrc-nrc.gc.ca*

John Luong

John H. Luong (PhD, 1979, McGill, Canada) is Head of Biosensors and Nanobiotechnology at the National Research Council Canada and the Walton Fellow at University College Cork, Ireland. His current research activities focus on biosensor technology, cell-based impedance spectroscopy, nanomaterials, electrochemical methods, capillary electrophoresis, and nanoscale analytical devices. He has received several awards and is the author and co-author of over 240 peer reviewed papers and several patents.

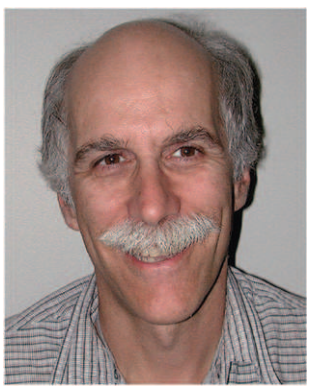

Keith Male

Keith B. Male (MSc, 1982, Carleton, Canada) is a Technical Officer in the Biosensors and Nanobiotechnology Group at the National Research Council of Canada. His laboratory experience is related to the development of biosensors for environmental and health applications, as well as the synthesis, characterization, functionalization and use of nanomaterials/nanocomposites such as metallic nanoparticles, carbon nanotubes and nanocrystalline cellulose. He has published over 80 peer reviewed papers.

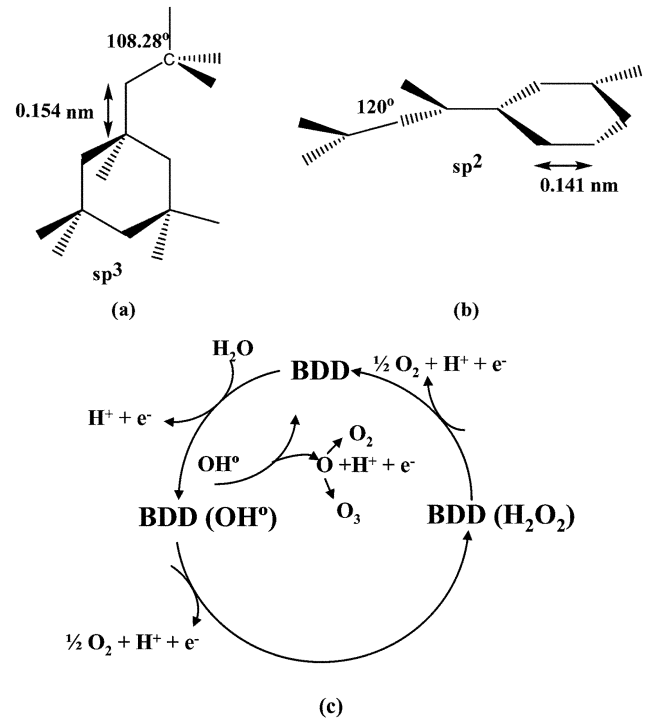

Fig. 1 (a) Robust crystalline structure of diamond with sp^3hybridization, (b) crystalline structure of graphite, sp^2 hybridization, and (c) hydroxyl radicals ($OH^{\bullet}$), known as the strongest oxidizing species, are produced in abundance at the anode as follows: $2H_2O \rightarrow 2OH^{\bullet} + 2H^+ + 2e^-$.

doped with other dopants to serve as electrode materials for diversified electrochemical applications. With such remarkable properties compared to graphitic carbon, BDD and two other novel carbon materials – fullerenes and carbon nanotubes – enable novel and/or improved applications in electronics, (bio)/electrocatalysis, and sensing technology. A distinct feature of BDD in electrochemistry, a very high overpotential for both oxygen and hydrogen evolution, was first reported by Pleskov *et al.*[3] The steady-state voltammetric response of the BDD electrode in 0.5 M H_2SO_4 at a scan rate of 0.1 V s^{-1} exhibits a wide potential window ranging from −0.75 to 2.35 V. This wide potential window (~3–3.5 V) can be extended to other electrochemical reactions in aqueous electrolytes.[4–11] High overpotentials of BDD are observed for halide[12,13] (I^-, Br^-, and Cl) oxidation and for the reduction of such corresponding halogens (I_2, Br_2, and Cl_2).[13] More detailed information of the electrochemical properties of BDD can be found elsewhere.[3]

Table 1 Comparison of the properties of CVD and natural diamonds

Property	CVD diamond	Single crystal diamond
Density, g/cm^3	2.8–3.51	3.515
Specific heat (C_p), at 300 K, J/mol	6.195	6.195
Thermal conductivity, at 25 °C, W/mK	2100	2200
Thermal expansion (10^{-6}/°C at 25–200 °C)	2.0	0.8–1.2
Refractive index at 10 μm	2.34–2.42	2.40
Band gap, eV	5.45	5.45
Electrical resistivity, Ω.cm	10^{12}–10^{16}	10^{16}
Dielectric constant (45 MHz–20 GHz)	5.6	5.70
Dielectric strength, V/cm	10^6	10^6
Loss tangent (45 MHz–20 GHz)	<0.0001	n.a.
Carrier mobilities (cm^2/Vs)	1350–1500	2200
Electron (n) Hole (p)	480	1600
Young's modulus, GPa	820–900	910–1250
Compressive strength, GPa		8.68–16.53
Poisson's ratio		0.1–0.16
Vickers hardness, GPa	50–100	57–104
Coefficient of friction in air	0.035–0.3	0.05–0.15

Noble metals such as platinum and gold with excellent chemical inertness have served as a workhorse in electrochemistry. However, the detection of various analytes in aqueous media is often not feasible at the high potential required for oxidation or reduction of such analytes, due to the high Faradaic currents produced by the oxygen and hydrogen evolution reactions. Mercury electrodes can circumvent this problem but they are not mechanically stable. The fabrication and replenishment of mercury is also problematical with respect to the generation of hazardous waste. The use of mercury has been banned in many countries throughout the world. Carbon-based materials such as graphite and glassy carbon might offer a large overpotential for the hydrogen evolution reaction but such electrodes are more vulnerable to surface oxidation and fouling. Almost all carbon surfaces of sp^2 hybridized materials react with oxygen and water to form oxygen-containing functional groups such as phenol, lactones, carbonyls, ethers, and carboxylates, known as surface oxides or simply oxides. The negative surface charge can have significant effects on adsorption, electron-transfer kinetics, and electrocatalysis. The interactions between the surface and adsorbate are governed by dipole–dipole interaction, induced dipoles, hydrophobic effects, electrostatic interaction, and covalent bonding. Therefore, they might require considerable surface cleaning and conditioning and are less suitable for long-term or *in situ* monitoring applications. In contrast, no oxide formation and reduction reactions between oxygen and hydrogen evolution occur on BDD surfaces (Fig. 1). BDD electrodes also possess very low capacitance and the largest potential window measured in aqueous electrolytes compared with conventional electrode materials including carbon-based and metallic electrodes.

Jeremy Glennon

Jeremy D. Glennon (PhD, 1979, University College Dublin, Ireland and PDF at the Research Institute. Hospital for Sick Children, Toronto, Canada) is Professor Chair of the Department of Chemistry at University College Cork, Ireland. His laboratory experience principally concerns the development of novel separation technology. He is actively involved in research, industrial training courses and in the teaching of analytical chemistry. He is the author and co-author of over 200 research and conference papers.

This review aims to provide a concise, up-to-date review covering the synthesis, surface modification and functionalization, electrochemical properties, and analytical applications using doped diamond electrodes. Their other applications including water treatment and electrosynthesis will not be covered and such information can be found elsewhere.[4,6]

Synthesis of doped diamond materials

As noted earlier, natural or undoped diamond with a bandgap of over 5 eV and resistivities in the order of 10^{20} Ω.cm is an electrical insulator and cannot be used as an electrode material. Albeit non-conducting diamond can be rendered conductive under vacuum annealing or surface transfer doping, diamond is often doped with boron, a low charge carrier with an activation energy of 0.37 eV, to form a p-semiconductor, known as boron-doped diamond (BDD).[14,15] The n-semiconductors can be prepared using phosphorus[16,17] (charge carrier activation energy 0.6 eV), nitrogen[15,17] (charge carrier activation energy 1.6–1.7 eV) or sulfur[17,18] as the dopant. Co-doped diamond thin films such as nitrogen–boron or boron–sulfur are also feasible since sulfur cannot be introduced in the absence of boron.[17,18] Four different types of diamond electrodes can be fabricated: (i) a doped diamond film deposited directly on a conducting substrate, (ii) an interlayer between the diamond film and the substrate, (iii) a doped diamond particle electrode, and (iv) diamond particles immobilized in an insulating layer (Fig. 2). Thermodynamically, unless the pressure is 15 000 times above atmospheric pressure, the spontaneous transformation of graphite to diamond is not feasible. Therefore, no serious attempt was made to grow diamond at low pressure before the 1980s. Nowadays, low-pressure chemical vapor deposition (CVD) diamond growth can be realized under appropriate activation conditions, such as activation by hot filament, low-pressure DC plasma, RF plasma or microwave discharge, hot DC or RF atmospheric pressure plasma, and even by combustion flames.

Chemical vapor deposition (CVD)

High pressure and high temperature (HPHT) grown diamond tends to consist of small crystals of a few millimeters in diameter. In 1962, Eversole[19] of the Union Carbide Corporation in the USA discovered that diamond could be deposited on a substrate from a hydrocarbon gas or CO/CO_2 mixture by CVD at low pressures and temperatures where diamond is a metastable phase with respect to graphite. However, this method only produces a very low yield of diamond. Since this important discovery, extensive research has been done on the CVD of diamond in the USA, Japan, Europe, and elsewhere. At room temperature and atmospheric pressure, graphite is the stable form of carbon with an enthalpy of 2 kJ mol^{-1} lower than diamond. For the diamond synthesis by CVD, it is imperative to deposit sp^3-bonded carbon and simultaneously suppress the formation of graphitic sp^2-bonds (Fig. 1). This can be realized by admixing large amounts of hydrogen to the process gas and by activating the gas either thermally or by plasma. Thus, all diamond CVD techniques are based on gas-phase non-equilibrium, using a high super saturation of atomic hydrogen with various hydrocarbon radicals. This plasma-assisted procedure uses hot filaments[4,7,20] or microwave radiation[21] to activate a gas phase at 2200–2800 °C. The latter is more convenient for the deposition of doped diamond on small surfaces whereas the former with multiple filaments is intended for larger substrates. In both cases, the gas phase held at ~10–50 mbar consists of a carbon source and hydrogen as the carrier gas, *e.g.* 0.5–3% methane in H_2 or acetone/methane mixture with boron as the dopant.[21] The hydrogen atoms in the plasma are used to terminate the carbon dangling bonds, which if allowed to reconstruct, will form sp^2 π-bonds, leading to graphite rather than diamond growth. Reduction of the hydrogen concentration while increasing the hydrocarbon content of the plasma causes the growth of non-diamond phases and an eventual decrease of the diamond phase. After activation, the plasma is deposited on a suitable substrate, maintained at 750–825 °C. The operating temperature also exhibits a significant effect on the reaction kinetics, particularly for endothermic methane decomposition. At high temperature, a high carbon flux in the gas phase is anticipated, *i.e.* the likelihood for sp^2-bonded carbon formation in the film. In contrast, the surface mobility of the carbon atoms is more sluggish at low temperatures. Hence, the number of open sites for diamond formation is lower, leading to the formation of more non-diamond phases. A comparison of the physical properties of natural diamond and CVD diamond is given in Table 1.

Microcrystalline diamond (MCD) *versus* nanocrystalline diamond (NCD)

Diamond films grown in hydrogen plasma are predominantly microcrystalline diamond (MCD) with grain sizes of

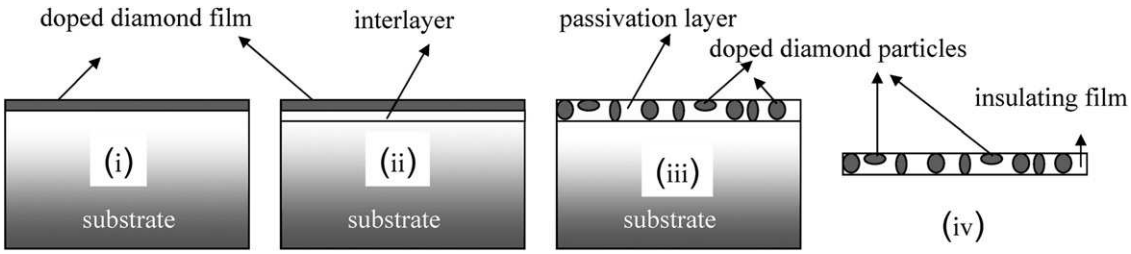

Fig. 2 Four different types of diamond electrodes: (i) doped diamond thin film without an interlayer between the substrate and diamond film, (ii) doped diamond thin-film electrode with an interlayer (often the corresponding metal carbide of the substrate), (iii) doped diamond particle electrode, in which particles are implanted in the conducting substrate with passivated surface, and (iv) doped diamond particle electrode, where particles are immobilized in an insulating film. The substrate indicated can be either single-crystalline or polycrystalline silicon, metals such as titanium, tantalum, tungsten, molybdenum and niobium or carbon-based materials such as graphite, glassy carbon or carbon fibre.

200–300 nm. The addition of 1% oxygen in a hydrogen plasma increases the grain size of diamond in the range of 300–550 nm. Until recently, MCD films were grown exclusively for wear resistance applications, so CVD using a CH_4/H_2 mixture appeared to fulfil this requirement. Fabrication of electronic devices or other applications requires much smoother surfaces, implying that the grain microsize must be reduced to nanoscale. Different techniques for growing nanocrystalline diamond (NCD) have been reported in the literature. The nucleation density can be increased further if diamond growth occurs on an MCD film synthesized using a methane concentration above 1.6%.[22] The film, however, still consists of NCD particles as well as graphite and amorphous carbon, and hydrogen plasma treatment (30 torr and 800 °C) is an effective way to remove such non-diamond and amorphous carbon phases. NCD films can be grown using the $Ar/H_2/CH_4$ plasma and the level of argon in the plasma is critical. Grain sizes of 60–2240 nm are obtained with argon contents ranging from 0 to 95% in the plasma. NCD films with very small grain sizes (<60 nm) are obtained in high argon content (>94%) in the plasma. In contrast, MCD with an average grain size of ~2240 nm is mostly formed with 60% argon in the plasma.[23] The surface of NCD has also significant π-bonding and sp^2 hybridization. Thus, NCD exhibits much higher conductivity than MCD and even undoped NCD is conductive.

Ultrananocrystalline diamond (UNCD) with fine grain size (3–5 nm) can be prepared from a hydrogen-poor deposition process.[24] The renucleation rate can be increased to the point where all columnar structure is lost by reducing the hydrogen concentration in the plasma. Unlike MCD or NCD, diamond films with nanoscale grain sizes are independent of the film thickness. Thus, UNCD does not grow in the standard van der Drift regime.[25] UNCD also possesses a very high grain boundary concentration (10%), thus electronic transport mechanisms become more complicated compared to classical infinite lattice-based band approximation. Nitrogen (0.02–10%) is useful for doping diamond to make it n-type. However, the conductivity is not due to doping, but can be attributed to the manipulation of the nanostructure of the material, leading to enhanced sp^2 regions and midgap states. The addition of diborane (300–2000 ppm) to the plasma makes the diamond films p-type as the boron dopes substitutionally and tends to congregate at the grain boundaries. UNCD displays low mobility hopping-type conduction and impurity band conduction, with very high carrier concentrations and low mobilities. Hence, UNCD can only be highly useful where high carrier concentrations are required, such as in electrochemical electrodes.

Single-crystalline or polycrystalline silicon and self-passivating metals including titanium, tantalum, tungsten, molybdenum, and niobium can be used as the substrate for diamond deposition. Other substrates are carbon-based materials such as graphite, glassy carbon, and carbon fiber. Regardless of the type of substrate used, the surface must be polished with diamond powder or ultrasonicated in a suspension of diamond nanoparticles.[7] Coating with diamond-like carbon on the substrate is another possibility. These resulting diamond crystallites on the substrate's surface are the nucleation sites for the growth of the thin diamond film during the subsequent CVD process. This is a prerequisite since diamond does not naturally nucleate on non-diamond substrates. Doped diamond films can be directly deposited onto silicon to form almost perfect and pore-free films (Fig. 2(i)). Silicon wafers, p-type (100), are often used as substrates for diamond film deposition. The silicon wafers are simply cleaned in a 2.5% HF solution to remove the native oxide layer. However, the brittleness of this substrate limits its use in many practical applications. With silicon and other chemically etchable substrates, the substrate can be removed by chemical etching to produce free-standing doped diamond films or even single-crystalline doped diamond.[26,27] Metal substrates are more favorable, particularly for the preparation of large-area electrodes, up to the square meter range. Niobium is best suited because it withstands high temperature and hydrogen-containing atmospheres. Nevertheless, large-area diamond electrodes based on silicon are prepared by a mosaic-like arrangement of diamond-coated silicon wafers on a metal substrate with subsequent passivation of the metal portions that are not protected by the silicon/doped diamond area. With metal substrates, an interlayer (*e.g.* the corresponding metal carbide) is often required to enhance the adhesion of the diamond film and protect the substrate against hydrogen in the deposition gas mixture (Fig. 2(ii)). Of interest is the embedding of Pt nanoparticles into the diamond film.[28] After growing a first diamond layer through CVD, Pt nanoparticles are sputtered onto the BDD layer, partially covering the surface. CVD is then resumed so Pt nanoparticles are sandwiched by the two diamond layers. The resulting electrodes consist of 10–500 nm Pt nanoparticles anchored within the BDD film. This approach results in a highly stable surface with Pt nanoparticles to serve as active catalysts for underpotential hydrogen deposition and alcohol oxidation.

The major structural effect of BDD is the presence of non-diamond carbon, mostly constituted by graphitic domains that could play the role of electrocatalytic centers and bring functional groups on the electrode surface. Such C-sp^2 impurities tend to be formed in the grain boundaries and defects during the CVD process.

High pressure and high temperature process (HPHTP)

This procedure is capable of implanting conducting diamond particles (100–200 μm) into conducting[29,30] or non-conducting substrates.[31] For the former, the space between the single diamond particles must be insulated by a non-conducting passivation layer of an inorganic or perfluorinated organic compound (Fig. 2(iii)). Non-conducting substrates must be very thin with the diamond particles facing both surfaces of the substrate.

Vacuum annealing and surface transfer doping

Thin, undoped diamond films prepared by microwave-assisted CVD become conductive after their annealation in a vacuum at above 1550 °C.[32,33] A conducting non-diamond carbon phase is formed along the intercrystalline boundaries leading to a conducting network. Some structural defects in the bulk of diamond crystallites also provide increased conductivity. The conducting phase is outcropped at the diamond film surface as an array of microelectrodes. The practical use of this procedure to prepare conducting diamond electrodes is somewhat limited. In a process termed '*surface transfer doping*',[34–37] hydrogen termination of the diamond surface results in a reduced ionization potential and

turns the diamond's electron affinity negative. Indeed, this phenomenon, high surface conductivity on an undoped hydrogenated diamond surface, was first reported by Landstrass and Ravi.[38] Undoped hydrogenated diamond can be doped by physisorbed surface adsorbates. Solvated ions in an aqueous and thin atmospheric layer can extract electrons from intrinsic diamond leaving behind holes as mobile charge carriers, resulting in a substantial surface conductivity with p-type conductivity. Diamond electrodes prepared by this method have been called surface conductive diamond (SCD) materials. The long-term stability of the surface transfer doping effect is very limited because this hydrogen-terminated surface can be easily changed to an oxygen-terminated surface during electrochemical processes, leading to attenuated electrical properties.

Surface characterization by Raman spectroscopy, scanning electron microscopy (SEM) and atomic force microscopy (AFM)

The grain size, surface morphology, and surface roughness of the polycrystalline diamond (PCD) films prepared from hydrogen-rich plasmas depend strongly on the film thickness. Generally, thick films possess large grain sizes with high surface roughness. C-sp^2 impurities tend to be formed in the grain boundaries and defects during the CVD process. Therefore, ultrananno-, nano- and poly-crystalline diamond layers are always dominated by grain boundaries which are decorated with C-sp^2 and amorphous carbon.[39–41] The volume fraction of sp^2 and grain boundaries is dependent on growth conditions and varies from layer to layer. UNCD might contain a high volume fraction of sp^2 up to 5%.[42] Surface morphology and crystal orientation of the microcrystalline diamond films depend on a variety of factors such as the nucleation rate and film deposition conditions. Such diamond films exhibit a significant surface roughness, 30–50 nm for NCD and from microns to tens of microns for polycrystalline layers. Commercial polycrystalline diamond is often mechanically polished to achieve a smooth surface and this step might cause some surface defects.

Scanning electron microscopy (SEM) can be used to probe the morphology of doped diamond films prepared by CVD such as grain size, orientation, and surface coverage.[43] A comparison of the SEM micrographs of nanocrystalline *versus* polycrystalline boron-doped diamond electrodes is shown in Fig. 3. Nowadays, both high quality nanocrystalline and polycrystalline BDD electrodes can be obtained from different commercial sources. For instance, high quality polycrystalline BDD electrodes are available from CSEM (Neuchatel, Switzerland). They are prepared by hot-filament chemical vapor deposition (HF-CVD) on 0.5 mm thick, 10 cm diameter silicon wafers, p-type doped to get a low resistivity (0.1 Ω.cm). The grain size varies from 200 to 800 nm. However, it is not known whether this film has been subjected to any mechanical polishing step. As produced, the average grain size of MCD can be up to ~1600 nm compared to ~40 nm for NCD, depending upon the growth conditions.[23]

Diamond morphologies include the {100} cubic, the {110} dodecahedral, the {111} octahedral, and other more complicated shapes.[1] Faceted grains are more or less obtained in the CVD diamond synthesis because of the tendency of the system to reduce its free energy by exposing the low surface energy planes. Such results are anticipated considering the conditions of CV synthesis: high temperature, low pressure, low methane flow rate, and low deposition rate. The theoretical surface energy per unit area of the {100}, {110}, and {111} facets is 1.124×10^{25} J m^{-2} mol^{-1}, 7.95×10^{24} J m^{-2} mol^{-1}, and 6.49×10^{24} J m^{-2} mol^{-1}, respectively. The {111} plane, with the lowest surface energy, is the preferred growth plane for CVD diamond.[1] Such features can be easily observed from the XRD pattern of the diamond film. Doped diamond films obtained from CVD exhibit different

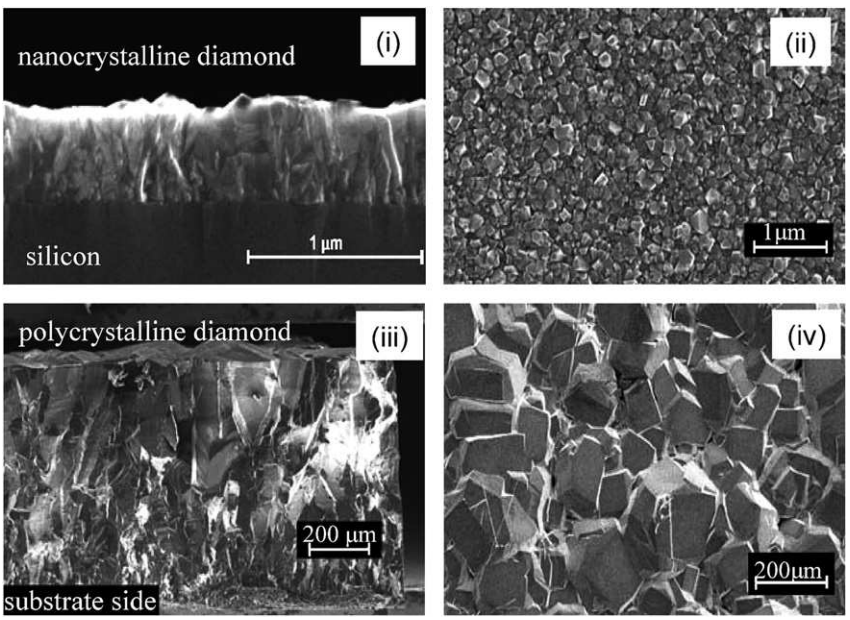

Fig. 3 Comparison of different diamond films. (Upper) Nanocrystalline diamond (NCD): (i) grain structure; (ii) surface morphology where the typical surface roughness is in the range of 30–50 nm. (Lower) Polycrystalline diamond (PCD): (iii) grain structure; (iv) surface morphology with a surface roughness of several tens of microns.

diamond crystal sizes (roughness) from 100 nm to 10 μm, different doping levels, and differing incorporation of graphitic and amorphous carbon. These factors affect the chemistry and performance of the electrode in different ways, and this flexibility opens the door for growing electrodes which are best suited to a diversified range of applications. It is possible to estimate the roughness of the BDD surface by atomic force microscopy (AFM) due to the high vertical resolution of this technique.[44] For the electrochemical deposition of Pt particles and clusters onto BDD thin films, AFM has been used to illustrate the existence of a small number of preferential diamond sites on which the initially deposited Pt particles are growing fast. The behavior might result from the high electrical conductivity near some sites, presumably due to a higher local concentration of boron used in the BDD films.[45]

Raman spectroscopy is another useful tool for characterization of diamond films as the genuine diamond displays only a single sharp peak at 1332 cm^{-1}, assigned to the diamond (sp^3-bonding) component.[46] Natural single crystal graphite exhibits a single G (graphite) peak at 1580 cm^{-1}, depicting the carbon–carbon stretching mode. When the graphite becomes disordered within the carbon layers, the 'G'-peak broadens and is slightly right-shifted (~1603 cm^{-1}). Polycrystalline graphite, depending on the size of the crystallites, might also display a second or D (disordered) peak at 1357 cm^{-1}. When the long range order of the crystalline material is lost and the carbon phase becomes glassy, both 'G' and 'D' are broadened, and the 'D'-peak intensity increases and downshifts. The Raman scattering cross-section of graphite is ~57 times larger than that of the characteristic diamond peak at 1332 cm^{-1} when using laser excitation at 514.5 nm. The penetration and escape depths of the laser and Raman scattered photons are significantly shorter in graphite (20 nm).[47] Thus, Raman spectroscopy is a useful tool to detect amounts of graphitic carbon in diamond films but is not a sensitive test for diamond in the presence of other types of carbon. Among others, rather a broad Raman band around 1150 cm^{-1} corresponds to NCD, which has been somewhat controversial, and ~1500 cm^{-1} to amorphous carbon. A further contribution to the spectrum is due to the fluorescence, which yields a background of increasing intensity with increasing wavenumbers. The hydrogen plasma sample often displays one sharp Raman peak at 1332 cm^{-1}, the diamond (sp^3-bonding) component. The high intensity of this peak with respect to the background fluorescence indicates good crystal quality. For the argon plasma sample, the typical diamond peak at 1332 cm^{-1} is significantly broadened whereas the Raman scattering intensity in the 1400–1600 cm^{-1} region is pronounced. Broadening of the diamond band might be caused by small grain size on the nanoscale, and the development of the 'graphite' band is due to increasing π-bonded carbon at the grain boundaries of the nanocrystalline films. In general, the intensity of the Raman peak at 1332 cm^{-1} for MCD is greater than that of NCD, indicating that the quality of MCD in terms of the sp^3-carbon content is better than in the NCD. The 1332 cm^{-1} peak of MCD has a FWHM of 8 cm^{-1}, compared with 24 cm^{-1} for NCD.[23] As the shape of the Raman spectra of diamond films might also depend on the excitation, the interpretation of Raman spectra of multi-component carbonaceous films might not be straightforward.[48–50] Therefore, X-ray photoelectron spectroscopy (XPS) should be used together with Raman to assess the high crystalline quality of CVD diamond since the presence of an sp^2-bonded carbon impurity (graphite peak) and the amorphous carbon peak should be detected at 26.50° and 33.96°, respectively.[51]

Modification of BDD surface

Surface modification by plasma treatment

The H_2 plasma used to make MCD by CVD automatically results in an H-terminated surface, which slowly reacts with oxygen. Conducting diamond under hydrogen plasma treatment will also result in a hydrogen-terminated surface.[52] To achieve hydrogen termination after growth, methane is switched off and the diamond is exposed to pure hydrogen plasma for a few minutes. Short oxygen plasma treatment leads to oxygen-containing functional groups on the diamond electrode surface[53,54] whereas its prolonged treatment results in a plasma etching of the diamond material to form a nanostructured diamond honeycomb film.[55] Fluorination of the diamond electrode surface, performed in an RF-plasma reactor under a CF–He-atmosphere within a few minutes results in a fluorine-terminated diamond surface with extraordinary hydrophobic properties.[55] Such materials exhibit a further increase of the hydrogen evolution overvoltage by over 1 V and consequently to a wider potential window (~5 V) in aqueous electrolytes.[56,57] Therefore, fluorinated diamond electrodes could be expected to be excellent cathodes for reactions that require very negative potentials, *e.g.* the electrodeposition of metals or nitrate reduction. Ammonia plasma treatment of hydrogen-terminated diamond electrodes resulted in doped diamond with surface terminal amino groups.[58] As addressed later, biomolecules can be covalently bound to such an amine-terminated moiety on the electrode's surface, and this type of diamond electrode could be useful for covalent attachment of biomolecules towards the development of various biosensing and biotechnological platforms.

Surface modification by chemical reactions

Chemical and electrochemical surface modifications of doped diamond electrodes have been attempted. Examples are the surface grafting of pyrenebutyric acid by esterification,[58] 2,4-dinitrophenylhydrazine,[58] 3-aminopropyltriethoxysilane (APTES),[59] quinone modification[60] and the covalent bonding of 4-nitrophenyl groups on single-crystalline diamond *via* the electrochemical reduction of 4-nitrobenzenediazonium tetrafluoroborate.[61] APTES-modified electrodes are of general interest and importance for diversified biosensing applications because such a terminal amino group can be used to immobilize biomolecules such as DNA, enzymes, receptors, *etc*. Of interest also is a photochemical modification scheme to fabricate H-terminated nanocrystalline diamond surfaces grown on silicon substrates. This homogeneous layer of amine groups can serve as a reaction site for DNA or other biomolecule attachment. Microcrystalline BDD thin films can be treated with a Piranha solution to produce a hydrophilic surface.[62] Although the procedure is reproducible, the resulting surface is only covered with a small fraction of a monolayer of hydroxyl functionalities. Nevertheless, this surface can be

reacted with adipoyl chloride in dry acetonitrile using 4-methylmorpholine as a Lewis base. The resulting terminal acid chloride functionalities can be reacted with 1-aminopyrene, a general scheme for subsequent attachment of biomolecules.

Deposition of thin films

Modification of diamond electrodes can be performed by the deposition of thin metal oxide films such as SnO_2,[63] cobalt oxide,[64] nanocrystalline ZnO,[65] and TiO_2.[66] In particular, cobalt oxide electrodeposited on doped diamond substrates results in electrodes with stable and high electrocatalytic performance for oxygen evolution. The deposition of cellulose on doped diamond can be performed by anodic electrodeposition from alkaline aqueous solution.[67] Cellulose-modified electrodes may be of interest in sensing/biosensing and for the protection of electrodes against interferences. In this context, a 'layer-by-layer' film of tyramine and pyrrole-1-propionic acid can be formed by subsequent electropolymerization on a BDD electrode with an overall thickness of ~33 nm.[68] The stable electropolymerized film is capable of excluding electroactive interference from L-DOPA, 3,4-dihydroxyphenylacetic acid, and ascorbic and uric acids at normal physiological conditions. The modified electrode can be used for several repeated analyses of dopamine without noticeable surface fouling. *N*-Acetyltyramine can also be electropolymerized together with a negatively charged sulfobutylether-β-cyclodextrin (SBCD) on a BDD electrode followed by the electropolymerization of pyrrole to form a stable and permselective film for selective dopamine detection with fast response time and low detection limit.[69] Glucose oxidase (GO) can be entrapped in an electrodeposited poly(tyramine) film together with a negatively charged SBCD on the active area of a platinum nanoparticle-modified BDD electrode.[70] The combined film of poly(tyramine) and SBCD serves as an excellent matrix polymer for the enzyme immobilization with high stability, selectivity, and reproducibility. Such a film is also capable of preventing the passage of electroactive uric and ascorbic acids to the electrode, two electroactive species which are commonly found in blood and other biological samples.

Ion implantation and electrodeposition

Metal ion implantation is a special technique to implant a metal species on a conducting diamond thin film, resulting in novel or improved electrocatalytic activities.[71–73] Conducting diamond thin films can be implanted with Ni^{2+}, Cu^{2+}, Pt^{2+}, or Ir^{+} ions. Ion implantation provides very small particles (usually in nanoscale) with high stability of distributed metal on the near surface of diamond. Nickel- and copper-implanted diamond electrodes can be used for the detection of glucose, platinum-implanted electrodes for hydrogen peroxide and iridium-implanted electrodes for As(III). Iridium oxide and platinum nanoparticles can also be deposited onto doped diamond by thermal decomposition of corresponding precursor solutions (*e.g.* H_2IrCl_6 or H_2PtCl_6 in isopropanol at 350 °C).[74,75] Metallic nanoparticles can be electrodeposited on a doped diamond substrate from their corresponding salts. The main purpose is to exploit the much higher catalytic activity of such nanoparticles using only very small amounts compared to the conventional bulk material. This approach has been attempted for IrO_2,[74,75] RuO_2,[76] gold,[77] platinum,[74,77] platinum/ruthenium,[74] platinum/tin,[78] copper[79] or cobalt[80] for various applications. Although this procedure is very simple and fast, long-term stability of such nanoparticles might not be sufficient and warrants further improvement.

Photochemical modification

Owing to its biocompatibility,[81–83] diamond has a potential for '*in-vivo*' biosensing applications. Biofunctionalization of its surface was a very difficult task until Takahashi *et al.*[84,85] introduced a photochemical chlorination/amination/carboxylation process of the initially H-terminated diamond surface. Based on this concept and the work of Wang *et al.*[86] and Zhang *et al.*,[87] a new photochemical method to modify NCD surfaces has become available.[88] This procedure involves the use of a long chain ω-unsaturated amine such as 10-aminodec-1-ene that has been protected with a trifluoroacetamide functional group (Fig. 4). The protected amine is then deprotected leaving a primary amine. Such a functionalized surface can then be used for covalent attachment of DNA, enzymes, proteins, and other biomolecules. For example, reacting the primary amine with a cross-linker followed by thiol-modified DNA will result in the attachment of DNA to the boron-doped diamond surface.

Electrochemistry of boron-doped diamond (BDD)

As noted earlier, diamond thin-film electrodes have been used increasingly in electrochemical studies because of their low background current, high current density electrolysis (1–10 A cm^{-2}), wide potential range, anti-adsorption, and high overpotential for oxygen evolution. In particular, a 5 V window of polarizability of fluorinated diamond electrodes in aqueous solutions is possible.[89] The conductivity of doped diamond electrodes is typically 500–10 000 ppm or 10^{19}–10^{21} atom cm^{-3}, depending on the doping level. With resistivities between 5 and 100 mΩ.cm, doped diamond also exhibits superconducting behavior at very low temperatures. Diamond electrodes are also different from conventional metal oxide electrode materials by their very low capacitance and by the absence of surface oxide formation and reduction reactions between oxygen and hydrogen evolution.

Thin-film diamond electrodes often possess some non-diamond sp^2-carbon impurities which can be deactivated by anodic oxidation in aqueous electrolytes. In cyclic voltammograms, the presence of sp^2-carbon impurities gives rise to an anodic current wave, starting before the oxygen evolution. This current peak rapidly diminishes with repeated scans and disappears from the third potential scan. The higher the sp^2-non-diamond carbon content the lower is the potential window between hydrogen and oxygen evolution in aqueous electrolytes. The hydrogen-terminated surface gives the electrodes a hydrophobic nature and could be stable for several months. However, the hydrogen-terminated surface is rapidly changed to an oxygen-terminated surface during anodic oxidation (*e.g.* oxygen evolution) in aqueous electrolytes. Oxygen-terminated diamond surface shows hydrophilic tendency and can be changed back to a hydrogen-terminated one by hydrogen flame or hydrogen-plasma treatment,[73] although it should be noted that some oxygen termination still remains. As noted earlier, C-sp^2-non-diamond

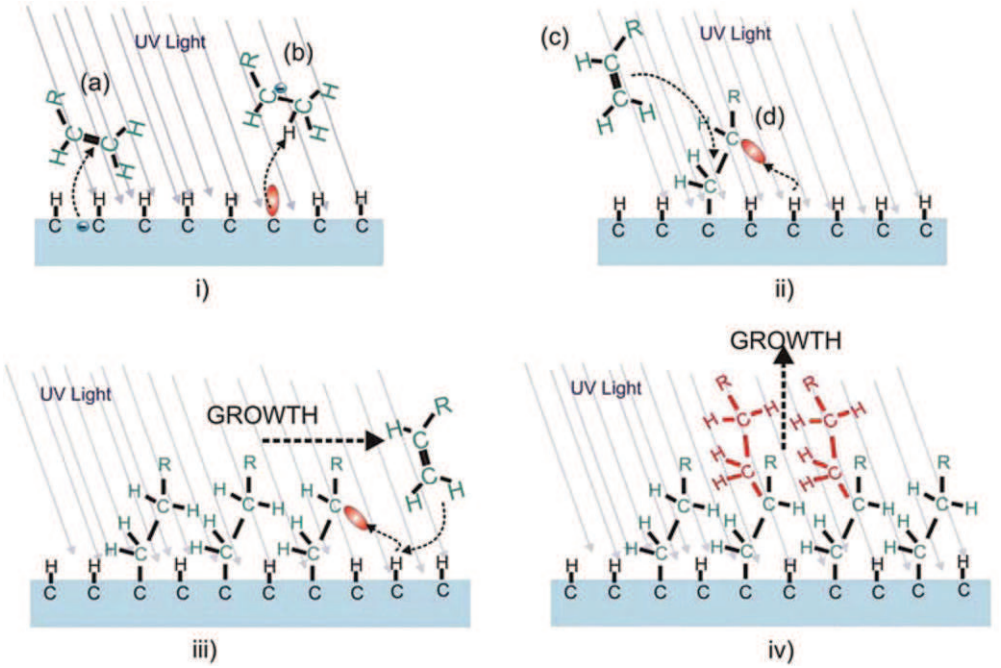

Fig. 4 Schematic grafting mechanism of the diamond surface by amines. (i) The generation of radical anions by electron transfer from diamond to the olefin (a). The nucleophilic properties of the radical cause a hydrogen abstraction (b) which results in a surface carbon dangling bond. (ii) Dangling bond reacts with an olefin molecule (c) to form a diamond–carbon/olefin–carbon bond. This olefin abstracts a hydrogen atom from the diamond surface (d) which is a new site for olefin addition. (iii) Hydrogen abstraction reaction results in a chain reaction. (iv) With extended illumination (>10 h), a 3D growth sets in due to cross-polymerization of olefin molecules. The 'R' represents a long chain ω-unsaturated amine, such as 10-aminodec-1-ene that has been protected with a trifluoroacetamide functional group.

active sites, often found in intercrystallite boundaries, electrochemically behave like edge planes of highly oriented pyrolytic graphite in nitric acid. Thus, these C-sp^2 active sites can be activated by anodic polarization at 1.7–1.8 V *vs.* Ag/AgCl in 1 M HNO_3 simultaneously to the deactivation of hydrogenated C-sp^3 active sites. The electroanalytical determination of the amount of C-sp^2 graphitic active sites is possible by cyclic voltammetry in 1 M HNO_3 since at least one oxidation peak and one reduction peak is observed. BDD materials are electrically heterogeneous with conductivity and electron-transfer rates varying across the BDD surface. This behavior is also confirmed by microscopic characterization of conductivity and redox activity for both hydrogen-[90] and oxygen-terminated[91] BDD electrodes.

Cyclic voltammetry is often used to study the electrochemical response of several doped diamond electrodes, with redox systems serving as probes: $Fe(CN)_6^{3-/4-}$, $Ru(NH_3)_6^{3+/2+}$, $IrCl_3^{3-/4-}$, $IrCl_6^{2-/3-}$, 4-methylcatechol, and $Fe^{3+/2+}$. The extent to which the physicochemical properties of glassy carbon (sp^2) and diamond (sp^3) carbon electrodes influence the response depends on the mechanistic aspects for the particular redox analyte. There are two types of reactions in heterogeneous electron transfer. The first type involves electrode reactions that proceed by simple mass transport of the analyte to the electrode–solution interface whereas the electrode simply serves as a source or sink for electrons. The electrode kinetics are relatively insensitive to surface chemistry and microstructure, but very sensitive to the density of electronic states close to the formal potential. The second type includes reactions that occur *via* some specific interaction with the electrode surface, *i.e.* reactions that proceed through an adsorbed state or involve some specific surface site. Besides the sensitivity to surface chemistry and microstructure, the electrode kinetics are also very sensitive to the density of electronic states near the formal potential. The test for 'surface sensitivity' can be attested if the rate constant (k^o, cm/s) remains constant regardless of whether the electrode surface is modified with a monolayer. The 'outer-sphere' or 'surface-insensitive' groups include $Ru(NH_3)_6^{3+/2+}$, ferrocene$^{+/-}$, anthracene$^{+/-}$, and $IrCl_3^{3-/4-}$.[92] They are considered to lack any electrocatalytic or adsorption step with low reorganization energy. Most conducting diamond materials have a lower density of electronic states than graphitic carbon and this factor might be attributed to slower kinetics for outer-sphere systems. Although the $Ru(NH_3)_6^{3+/2+}$ redox couple shows classical voltammetric waves, similar to those obtained by glassy carbon, the rate constant (k^o, cm/s) of MCD[93] is much slower (0.012–0.017 compared to 0.51 for glassy carbon (GC-20))[94] whereas a considerably higher value for k^o (0.1 cm/s) is reported for nitrogen-doped NCD.[95] As noted earlier, for polycrystalline diamond, a background oxidation is commonly observed at +1.83 V on the first scan. Such a result can be attributed to the irreversible oxidation of sp^2 impurities along grain boundaries owing to the presence of ionizable surface carbon–oxygen functional groups, *e.g.* carboxylic acid. The voltammetric responses for $Fe(CN)_6^{3-/4-}$ and $Ru(NH_3)_6^{2+/3+}$ on MCD and NCD reveal the absence of electrostatic double layer effects which are commonly observed for sp^2-carbon electrodes. Heterogeneous electron-transfer rate constants (k^o) of 0.01–0.2 cm/s are typical for both conducting microcrystalline and nanocrystalline films without extensive pretreatment.

In contrast, extensive pretreatment is normally required to activate sp^2-carbon and metal electrodes for charge transfer. Cyclic voltammograms of a platinum and hydrogen-terminated boron-doped diamond electrode with the redox couple $Fe(CN)_6^{3-/4-}$ are somewhat comparable although platinum is more reversible.[96] The doping level and pretreatment of the diamond electrode play an important role on the kinetics of charge transfer reactions. For example, the surface interactions appear to be blocked on oxygen-terminated BDD surfaces.

More irreversible behavior of diamond electrodes, especially at low doping levels and with oxygen-terminated surfaces, is often encountered. CF-BDD electrodes (diamond formation on carbon felt substrates) also exhibit quasi-reversible behavior: the separation between the anodic and cathodic peaks (ΔE_p) is larger than $59/n$ mV (where $n = 1$ is the number of electrons involved in the reaction) and increases with sweep rate (v) increase; current peak intensity (I_p) increases with $v^{1/2}$ increase, but does not keep proportionality; and the cathodic peak potential (E_{pc}) shifts to negative values, with v increase. The I_{anp}/I_{cathp} peak ratio could be up to 1.6, far from the expected value of unity for reversible kinetics. The current peak (I_p) has also been related to the sweep rate (v, scan rate) as I_p *vs.* v^{γ} where γ is related to the fractal dimension (FD): $FD = 2\gamma + 1$. The FD values (2.3–2.5, *i.e.* $\gamma = 0.65$–0.75) measured by cyclic voltammetry are in agreement with AFM.[97] BDD films might present a FD value below 2 instead of 2.5 for non-doped diamond films, suggesting non-contiguous electrochemical active sites for the ferrocyanide redox reaction and the reaction might occur at the summit hill.

In non-aqueous electrolytes such as propylene carbonate,[98,99] acetonitrile,[99,100] γ-butyrolactone, *N*,*N*-dimethylformamide, diethyl carbonate/propylene carbonate mixtures, and methanol,[99] BDD film electrodes exhibit a 1.5–2.5 times wider potential window (~5.0–7.5 V) than in aqueous electrolytes. However, this feature is not unique to BDD since glassy carbon or graphite electrodes also exhibit similar electrochemical behavior in such organic media.

Analytical applications of BDD electrodes

In (bio)sensing applications, both pristine and modified diamond electrodes can be used, depending on the specific analyte. The main push for BDD electrodes is their low capacitive current, leading to an enhanced signal to noise ratio (S/N). The large potential window also opens up several important applications which could not be accomplished with conventional electrode materials. Low adsorption of contaminants leads to low fouling and this feature is very important for an extended use. Therefore, BDD electrodes exhibit high stability, high sensitivity, and a low detection limit. Diamond electrodes can be modified by nanoparticles *via* ion implantation or electrodeposition. The advantageous properties of the electrodes are their inherent stability with very low background currents.

Several electroanalytical techniques have proven very useful with doped diamond electrodes: amperometric detection, anodic stripping voltammetry (ASV), cathodic stripping voltammetry (CSV), abrasive stripping voltammetry (AbSV) and square wave voltammetry (SWV). The target analyte can be an organic compound or an inorganic species including metal ions. In particular, the analysis of trace hazardous metals such as lead, cadmium, mercury, arsenic, thallium, selenium, *etc.*, is of importance due to growing concerns about their toxicity in drinkable water and foodstuffs. For such metals, the detection limit must be down to parts-per-billion or even parts-per-trillion due to their very low presence in a variety of matrices including air, water, and soil, as well as in physiological tissues and fluids. Electrochemical stripping analysis together with doped diamond electrodes might be an attractive, powerful tool for detecting trace metals. Electrochemical oxidation of such analytes might form a continuous conductive film on BDD with 2′-deoxyguanosine as a typical example.[101] For the detection of phenol, the oxidized products might depend on the applied potential. As an example, for the oxidation of pentachlorophenol (PCP) on BDD electrodes at 0.9 V, the formation of an adherent film on the electrode surface involves the transference of one electron per PCP molecule and the film is identified as the dimer 2,3,4,5,6-pentachloro-4-pentachlorophenoxy-2,5-cyclohexadienone. At +2.0 V, the formation of the corresponding quinone (*p*-tetrachlorobenzoquinone) is detected at the beginning of the process.[102] Various anions, metals, and organic compounds have been analyzed by BDD electrodes (Table 2 and Table 3).[72,74,103–149] Amperometric detection can be performed with flow injection analysis (FIA), HPLC, and capillary electrophoresis (CE) including the CE chip (Table 4).[73,103,104,107,121,141,142,145,147–156]

The application of diamond microelectrodes and microelectrode arrays is indeed an interesting feature and the use of biomolecules as specific sensing elements together with doped diamond electrodes to impart selectivity has emerged for analysis of the target analyte in 'real world' samples. The first important step is the immobilization of such biomolecules on the active area of the BDD electrode. The inertness of BDD electrodes is beneficial in terms of electrode stability; however, it may limit the biosensing applications of diamond thin films since a pertinent biomolecule must be covalently attached to the electrode's surface to impart selectivity. Nevertheless, several bio-functionalization procedures have been developed as discussed earlier and applications of BDD electrodes with immobilized biomolecules have emerged (Table 5).[70,132,138,157–170]

Functionalized nanocrystalline diamond (NCD) can be used to effect direct electron transfer between the redox center of the enzyme and the NCD surface. In this context, horseradish peroxidase (HRP) was immobilized on the surface of functionalized NCD thin films to allow direct electron transfer between them due to the proximity of HRP heme groups to the NCD surface.[171] Direct electron transfer has also been reported for glucose oxidase covalently immobilized on an oxidized boron-doped diamond electrode which possesses carboxyl groups.[172] However, the detection limit for glucose is only 23 μM, considerably lower than with the detection scheme using carbon nanotubes and platinum nanoparticles to effect direct electron transfer.[173] It remains to be seen whether this approach can be improved and/or extended to other important enzymes which have been widely used in biosensing with sufficient detection sensitivity and stability.

Conclusions and outlook

Conducting diamond with exceptional hardness, inertness and stability has been proven as a versatile electrode material for the

Table 2 Analysis of inorganic ions and metal ions

Analyte	Some important remarks
Azide anion[103–105]	Hydrogen-terminated BDD, LOD = 8 nM in physiological buffers
Hydrazine[106]	Palladium nanoparticles on BDD, LOD = 2.6 μM
H_2O_2[72]	Platinum-modified BDD, LOD = 30 nM
Iodide[107]	LOD = 10 nM using nuclear emergency tablets
Nitrate[108]	Copper nanoparticles on BDD, LOD = 1.5 μM in mineral water
Nitrite[104]	LOD = 7 nM
Dissolved oxygen[74]	IrO_2 and gold nanoparticles (NPs), Pt NPs or Pt/Ru NPs on BDD
Dissolved ozone[109]	LOD ≈ 300 ppb with a slope of 6.7 μA cm^{-2} (mg $L^{-1})^{-1}$
Peroxodisulfate[110]	LOD = 5 ppt
Sulfate[110]	LOD = 5 ppt
Sulfide[111]	BDD microelectrode array, LOD = 23 μM
Ag^{+} [112–115]	Detection using abrasive stripping voltammetry (AbSV) or anodic stripping voltammetry (ASV) with LOD = 10 ppb
As(III)[116,117]	Pt nanoparticle-modified BDD with LOD = 0.5 ppb; electrochemical etching of Pt allowed reuse of microelectrode 150 times
Cd^{2+} [114,115,118]	LOD = 1 ppb comparable to Hg-glassy carbon electrodes. Sensitivity improved by ultrasound to nM detection
Cu^{2+} [113,115,119]	LOD = 1 ppb using ASV
Hg^{+} [120,121]	Differential pulse voltammetry (DPV) is performed in nitrate, thiocyanate and chloride media (most samples usually contain chloride impurities). The formation of calomel in a chloride medium on the BDD surface is avoided by the co-deposition of purposely-added gold (3 ppm) during DPV detection. Mercury in the 0.005–50 ppb range can be detected using a rotating disk electrode (RDE) technique
Mn^{2+} [111,122]	LOD = 10 pM using ultrasound-assisted cathodic stripping voltammetry (CSV). Tested in tea samples
Ni^{2+} [123]	LOD = 100 nM with CSV
Pb^{2+} [113–115,119,124–125]	LOD = 5 ppb with ASV. Simultaneous detection with Cu^{2+} at 2 nM
Sn^{4+} [112]	Abrasive stripping voltammetry
Zn^{2+} [113,115]	LOD = 100 ppb (ASV)

Table 3 Analysis of organic compounds

Analyte	Some important remarks
Adenosine[126]	LOD = 10 nM *in vitro* using BDD microelectrode. Used to investigate respiratory rhythmogenesis
Ascorbic acid[104]	LOD = 12 nM
Caffeine[127]	LOD = 1–400 μM
Carbamate pesticides[128]	LOD = 5–20 ppb, lowered to 0.6–1.0 ppb by alkaline hydrolysis pretreatment
Catechols[104]	LOD = 2 nM for 4-methylcatechol
Cephalexin[129]	LOD = 5 μM
Chlorophenols[130]	LOD = 5.5 ppb in pure water and 15.5 ppb in polluted water for pentachlorophenol. Detection range of 1–250 μM for 4-chorophenol using a tyrosinase-immobilized BDD electrode
Chlorpromazine[10]	LOD = 4 nM
p-Cresol[132]	Detection range of 1–200 μM using a tyrosinase-immobilized BDD electrode
Cysteine[133]	LOD = 100 nM using FIA
Dopamine[134]	LOD = 50 nM using As-deposited BDD
Formaldehyde[135]	Under neutral conditions, detection range of 50–600 μM
Glucose[136]	Ni- and Cu-modified BDD for glucose detection by FIA. LODs of 670 nM and 1.5 μM, respectively. Low background noise much better than bare Ni or Cu
Glutathione[129,137]	LOD = 10 μM, but down to 500 nM using FIA
Histamine[138]	LOD = 500 nM
Indoles[120]	LOD = 50 μM for tryptophan, 1-methylindole and indole 3-methanol
NADH[134]	LOD = 10 nM
Nitrophenol[111,139]	LOD = 2.8 ppb for 4-nitrophenol. Advantageous for waste water samples compared to hanging mercury drop electrode
Nucleic acids[140]	Detection of dGMP, tRNA, ssDNA, and dsDNA by SWV, signal related to guanosine groups
Oxalic acid[141]	LOD = 0.5 nM using hydrogen-terminated BDD
Penicillamine[142]	LOD = 10 nM with FIA
Phenol[132]	Detection range of 1–200 μM for phenol using a tyrosinase-immobilized BDD electrode
Polyamines[143,144]	LOD = 1 μM with dynamic range up to 1 mM for ethylenediamine, putrescine, spermine, cadavarine, and spermidine
Purines and pyrimidines[145]	Measured in DNA samples with HPLC separation. Detection limits of 162 nM (cytosine), 35 nM (guanine), 106 nM (thymine), 26 nM (adenine) and 82 nM (5-methylcytosine)
Serotonin[138,146]	LOD = 10 nM using polycrystalline BDD thin-film electrodes. LOD = 1 nM using BDD on tungsten microelectrodes to measure feeding patterns of *Aplysia californica* as function of serotonin concentration
Sulfa drugs[147]	LOD = 50 nM
Tetracycline[121,148]	LOD = 10 nM using anodized BDD and FIA
Theobromine, theophylline[127]	Detection range of 1–400 μM
Tiopronin[149]	LOD = 10 nM in pharmaceutical formulations
Xanthine[127]	Detection range of 1–100 μM

Table 4 Detection schemes using flow injection analysis, HPLC or capillary electrophoresis (CE)-CE chips

Analyte (detection limit)	Some important remarks
FIA	
Arsenite (As^{III})[73]	Iridium-modified BDD by ion implantation method, LOD = 20 nM or 1.5 ppb using spiked tap water containing Al, Fe, Mn, Cl, Ca, Mg, and NO_3
Azide[103]	LOD = 8 nM or 0.3 ppb
Cadaverine, putrescine, spermidine and spermine[144]	LOD = 1.0 μM and 0.32 μM for spermine
Chlorpromazine[104]	LOD = 4 nM
Ferrocyanide, ferricyanide[150]	LOD = 570 nM
Iodine[107]	LOD = 10 nM in nuclear emergency tablets
Oxalic acid[141]	Hydrogen-terminated BDD, LOD = 0.5 nM
Penicillamine[142]	LOD = 10 nM in pills
Tetracycline[148]	Anodized BDD, LOD = 10 nM
Tiopronin[149]	LOD = 10 nM in pharmaceutical formulations
HPLC	
Polycyclicaromatic hydrocarbons (PAHs)[151]	LOD = 12–40 nM for 16 EPA priority compounds
Sulfonamides[152]	FIA/HPLC coupled with amperometric detection using boron-doped diamond, LOD = 11 ppb, egg samples
Tetracyclines[145]	Anodically oxidized BDD, LOD = 26–162 nM. Detection of 5-methylcytosine in DNA samples
Sulfa drugs, sulfadiazine, sulfamerazine and sulfamethazine[147]	LOD = 50 nM
Tetracyclines[121]	Nickel-implanted BDD, LOD = 10–50 ppb, analysis in shrimp samples
Amperometric detection of oxidized and reduced glutathione (GSH and GGSG)[153] and homocysteine[154] using a BDD electrode after an HPLC column	The analysis of GSH and GSSG is performed in Britton–Robinson buffer at pH 2. The glutathione is detected in an aqueous acidic media (pH 2) containing 2% acetonitrile in 0.05 M phosphate buffer. The detection limits are 1.4 nM for GSH, 1.9 nM for GSSG and 1 nM for homocysteine
CE-CE chips	
Guanosine[155]	LOD ≈ 1 μM using microchip CE with BDD detection
Nitroexplosives, phenols and organophosphate nerve agents[156]	A BDD film band (0.3 × 6 mm) for end-column amperometric detection. LOD = 70 ppb for 1,3-dinitrobenzene

detection of a myriad of important analytes with low detection limits, excellent precision and stability. Another important feature is the stabilization time (the time required for the background current to attain a stable and steady value) of BDD electrodes, which is within 2 min compared to 10–14 min for glassy carbon electrodes at phosphate pH 7. However, aqueous basic conditions must be avoided because these conditions result in degradation of the diamond surface. BDD electrodes can function in aggressive solution environments without any microstructural or morphological degradation. Therefore, they may find significant applications where stability is paramount, *e.g. in situ* monitoring. Another promising area of BDD is micro- or nano-structuring of thin films and their surfaces. There are several commercial sources that market conducting diamond thin-film electrodes with affordable cost. Microarrays can also be fabricated entirely from diamond with an average surface roughness below ±10 nm over the array.[174] A BDD microelectrode array can also be micromachined using microwave-induced plasma growth and laser ablation shaping techniques.[175] The active BDD element can be tuned to between 10 and 50 μm in diameter with a 10 times diameter center-to-center distance between two adjacent conducting elements. Such a device should foster applications in harsh conditions such as high temperature, high pressure, and resistive media under dynamic flow regimes.

The electron cyclotron resonance (ECR)-sputtered carbon film can be deposited within several minutes at room temperature.[176] The optimized sputtering conditions significantly change the film structure, which includes many more sp^3-bonds (sp^3/sp^2) = 0.702 than a previously reported film (sp^3/sp^2) = 0.274 with an extremely flat surface (0.7 Å). The ECR-sputtered carbon films exhibit nearly the same potential window in the positive direction as that of boron-doped diamond (moderately doped, 1019–1020 boron atoms cm^{-3}) and an even wider potential window in the negative direction with a low background current. The ECR-sputtered carbon film is advantageous for measuring biochemicals with high oxidation potentials because of its wide potential window and high stability. However, they are much slower than those of glassy carbon for $Fe^{2+/3+}$, dopamine oxidation, and O_2 reduction due to weak interactions between electroactive species and the ECR-sputtered carbon film surface, attributed to the ultraflat surface and low surface O/C ratios of ECR-sputtered carbon films.

There is a plethora of opportunities for nanoscale devices based on conducting diamond. With favorable mass transport, nanoscale devices enable the study of very fast electrode kinetics and enhance the response of many electroanalytical sensors. As an example, conventional graphitic and glassy carbon electrodes cannot detect lanthionine ketimine (LK) and its derivatives whereas boron-doped diamond electrodes have been capable of detecting LK and LK esters. Huntington's disease is believed to damage nerve cells through inflammation, excess nitric oxide production, and excess glutamate excito-toxicity. LK has shown the potential to stop damage to nerve cells and reduce inflammation.[177] Exotic electroanalysis is the use of BDD electrodes for the detection of heavy metals such as Ag(I), Pb(II), and Cd(II) in the International Space Station water. Surprisingly, the latter

Table 5 Biosensing applications with BDD electrodes

Target analyte	Some special remarks
Phenolic compounds[132]	Tyrosinase is immobilized *via* a layer of amino groups
Direct biocatalysis of the dioxygen reduction – biofuel cell application[157]	BDD activated by anodic oxidation is a highly active material, providing intimate contact of laccase enzyme molecules with the electrode surface
Hydrogen peroxide[158]	Immobilized catalase
A field-effect biosensor[159]	Immobilized DNA oligonucleotides
Glucose[70]	Immobilization of glucose oxidase in an electropolymerized film on a platinum nanoparticle-modified BDD electrode
Sequence-specific DNA using copper-enhanced anodic stripping of purine bases[160]	The novel use of electrochemistry to generate covalent oxidative labels on intact proteins. BDD as a useful tool for conducting oxidative surface mapping experiments
Stripping voltammetric determination of purine bases in the presence of copper ions[161]	An easy detection of ~25 fmol of the oligodeoxynucleotides. Suitable for determination of purine (particularly guanine) content in DNA samples
In vivo detection of dopamine in mouse brain[162]	BDD microelectrodes (~5 μm in diameter and 250 μm in length) were fabricated and inserted into the corpus striatum of the mouse brain. The sensors displayed good sensitivity and stability
Mouse IgG (MIgG)[163]	*o*-Aminobenzoic acid (*o*-ABA) is electropolymerized at a BDD electrode by cyclic voltammetry. An antimouse IgG from goat (GaMIgG) is covalently immobilized at a poly-*o*-ABA-modified BDD electrode which used a sandwich-type alkaline phosphatase catalyzing amperometric immunoassay with 2-phospho-L-ascorbic acid as substrate. LOD = 0.30 ng mL^{-1} compared to 3.50 ng mL^{-1} for MIgG at a glassy carbon (GC) electrode. The dynamic range of the modified BDD electrode is about 3 orders of magnitude (1–1000 ng mL^{-1}) compared with the modified GC (10–500 ng mL^{-1})
Detection of conformational changes in large, non-metalloproteins such as bovine serum albumin (BSA)[164]	FIA is coupled with hydrogen-terminated, BDD electrodes. The oxidation current is used as a signal reporter in the monitoring of urea-induced BSA denaturation. The oxidation involves at least five redox-active species (cysteine, tryptophan, tyrosine, methionine, and disulfide bonds). LOD = 190 ng mL^{-1} is achieved for BSA
Differentiation of gene sequences according to DNA hybridization events without labeling[165]	BDD electrodes are dipped into a 1% solution of polyethyleneimine (PEI) to adsorb a thin layer of positively charged PEI. PEI-modified BDD electrodes are used to immobilize negatively charged single-stranded PCR fragments from Exon 7 of human *p53* gene. Alternating current impedimetric measurements are first performed on these systems in phosphate buffered saline and upon exposure to single-stranded DNA (ssDNA). Complementary DNA can be detected at 10^{-19} g mL^{-1}
Real-time detection of changes in histamine over the oxyntic glands of guinea pig stomach[166]	The BDD microelectrode is used in an amperometric mode to detect histamine when the electrode is placed over the tissue. The electrode provides stable and reproducible responses, qualitatively consistent with the signaling mechanism for acid secretion at the stomach. When the H_2 receptor antagonist cimetidine is perfused to the tissue, histamine levels increase, resulting in an increase in the response signal. Addition of acetylcholine (ACh) decreases the signal response, indicating that the primary influence of ACh is directly on the parietal cell receptors rather than the enterochromaffin-like cell receptors of the oxyntic glands
NADH detection and enzyme-catalyzed reactions involving NADH as a cofactor[167]	Highly reproducible cyclic voltammograms for NADH oxidation are obtained at As-deposited diamond electrodes. With a detection limit of 10 nM, the response signal is stable over several months of storage in ambient air, in contrast to glassy carbon electrodes, which are deactivated within 1 h. An NADH-mediated dehydrogenase-based ethanol biosensor incorporating an unmodified diamond electrode is demonstrated
Detection of histamine and serotonin in neutral aqueous media, pH 7.2[138]	Polycrystalline, boron-doped diamond thin-film electrodes are used to study the oxidation reactions of histamine and serotonin. A detection limit of 0.5 μM for histamine is obtained by use of the FIA technique with a diamond electrode. A remarkably low detection limit (10 nM) is obtained for serotonin
Detection of *Escherichia coli* in foodstuffs[168]	*o*-Nitrophenol, released from *o*-nitrophenyl-β-D-galactopyranose as catalyzed by β-galactosidase, a tetramer of *E. coli*, is exploited for the detection of *E. coli* contamination in foodstuffs. This reaction can be detected using an unmodified boron-doped diamond electrode poised at +0.93 V. The detection limit is 4×10^4 cells mL^{-1} with a total analysis time of <1.5 h
Scanning electrochemical microscopy using a BDD ultramicroelectrode (1–25 μm) for imaging of respiring *E. coli*[169]	BDD films are deposited by chemical vapor deposition onto sharpened tungsten wires. The sensing tip is insulated by nail varnish, electrophoretic paint and fast-setting epoxy. The tip is applicable for electrochemical imaging in biological media

Table 5 (*Contd.*)

Target analyte	Some special remarks
Detection of dopamine and uric acid using a BDD nanograss array[170]	A BDD nanograss array (20 nm diameter, 200 nm length) was prepared on a heavily doped BDD film by reactive ion etching using oxygen plasma. A detection limit of 0.8 μM for dopamine was achieved and selectivity over uric acid was enhanced due to the surface's ability to change the reactive sites. The arrays were stable and could be used for repeated analysis after simple sonication, unlike other modified electrodes

two were found at concentrations much higher than the US Environmental Protection Agency action levels.[178]

Boron-doped diamond thin films can be considered as one of the most ideal electrode materials for electroanalysis and electrolysis. BDD will occupy a special place as an electrode material in biosensing applications. Several important areas of future work include chemical modification of diamond surfaces to control adsorption and charge transfer kinetics and patterning diamond electrodes into microarray configuration. The mechanisms underlying the differences in the surface conductivities for the hydrogen- and oxygen-terminated BDD surfaces remain unclear. These mechanisms warrant further investigation in order to foster the utilization of surface properties of diamond in electroanalysis and biosensing applications.

Acknowledgements

This work was supported by the Science Foundation of Ireland, the Walton Visitor Award (J. H. T. L.).

References

1 H. Lin and D. Dandy, in *Diamond Chemical Vapor Deposition, Nucleation and Early Growth*, Noyes Publications, New Jersey, 1995, p. 2.
2 A. T. Collins, P. J. Dean, E. C. Lightowler and W. F. Sherman, *Phys. Rev.*, 1965, **140**, A1272–A1274.
3 Y. V. Pleskov, A. Y. Sakharova, M. D. Krotova, L. L. Bouilov and B. P. Spitsyn, *J. Electroanal. Chem.*, 1987, **228**, 19–27.
4 F. Beck, H. Krohn, W. Kaiser, M. Fryda, C. P. Klages and L. Schafer, *Electrochim. Acta*, 1998, **44**(2–3), 525–532.
5 M. Panizza and G. Cerisola, *Electrochim. Acta*, 2005, **51**, 191–199.
6 M. A. Q. Alfaro, S. Ferro, C. A. Martínez-Huitle and Y. M. Vong, *J. Braz. Chem. Soc.*, 2006, **17**, 227–236.
7 M. Fryda, T. Matthee, S. Mulcahy, A. Hampel, L. Schafer and I. Troster, *Diamond Relat. Mater.*, 2003, **12**, 1950–1956.
8 H. B. Martin, A. Argoitia, U. Landau, A. B. Anderson and J. C. Angus, *J. Electrochem. Soc.*, 1996, **143**, L133–L136.
9 N. Katsuki, E. Takahashi, M. Toyoda, T. Kurosu, M. Iida, S. Wakita, Y. Nishiki and T. Shimamune, *J. Electrochem. Soc.*, 1998, **145**, 2358–2362.
10 B. Marselli, J. Garcia-Gomez, P.-A. Michaud, M. A. Rodrigo and C. Comninellis, *J. Electrochem. Soc.*, 2003, **150**, D79–D83.
11 F. Beck, W. Kaiser and H. Krohn, *Electrochim. Acta*, 2000, **45**, 4691–4695.
12 M. Swain, A. B. Anderson and J. C. Angus, *MRS Bull.*, 1998, **23**(9), 56.
13 N. Vinokur, B. Miller, Y. Avyigal and R. Kalish, *J. Electrochem. Soc.*, 1996, **143**, L238–L240.
14 A. Fujishima, Y. Einaga, T. N. Rao and D. A. Tryk, in *Diamond Electrochemistry*, Elsevier, Amsterdam, 2005.
15 W. Haenni, P. Rychen, M. Fryda and Ch. Comninellis, in *Thin-Film Diamond Part B*, ed. C. Nebel, Semiconductors and Semimetals Series, Academic Press, Elsevier, Amsterdam, 2004, p. 149.
16 M. Nesladek, *Semicond. Sci. Technol.*, 2005, **20**, R19–R27.
17 S. C. Eaton, A. B. Anderson, J. C. Angus, Y. E. Evstefeeva and Y. V. Pleskov, *Electrochem. Solid-State Lett.*, 2002, **5**, G65–G68.
18 S. Vaddiraju, S. Eaton-Magana, J. A. Chaney and M. K. Sunkara, *Electrochem. Solid-State Lett.*, 2004, **7**, G331–G334.
19 W. G. Eversole, *US Pat.*, 3030187, 1962; W. G. Eversole, *US Pat.*, 3030188, 1962.
20 L. Schäfer, M. Höfer and R. Kröger, *Thin Solid Films*, 2006, **515**, 1017–1024.
21 T. Yano, D. A. Tryk, K. Hashimoto and A. Fujishima, *J. Electrochem. Soc.*, 1998, **145**, 1870–1876.
22 K. Kobashi, K. Nishimura, K. Miyata, K. Kumagai and A. Nakaue, *J. Mater. Res.*, 1990, **5**, 2469–2482.
23 R. Ramamurti, Ph.D. Thesis, University of Cincinnati, 2006.
24 D. M. Gruen, *Annu. Rev. Mater. Sci.*, 1999, **29**, 211–259.
25 A. van der Drift, *Philips Res. Rep.*, 1967, **22**, 267–288.
26 H. B. Martin, A. Argoitia, J. C. Angus and U. Landau, *J. Electrochem. Soc.*, 1999, **146**, 2959–2964.
27 J. van de Lagemaat, D. Vanmaekelbergh and J. J. Kelly, *J. Electroanal. Chem.*, 1999, **475**, 139–151.
28 J. Wang, G. M. Swain, T. Tachibana and K. Kobashi, *Electrochem. Solid-State Lett.*, 2000, **3**, 286–289.
29 W. Wesner, M. Kotschan, R. Hermann, W. Staber and M. Schelch, *Int. Pat. Appl.*, WO 2004/00558.
30 A. Cieciwa, R. Wüthrich and C. Comninellis, *Electrochem. Commun.*, 2006, **8**, 375–382.
31 K. Gruber, *Int. Pat. Appl.*, WO 2005/116302.
32 Y. V. Pleskov, M. D. Krotova, V. G. Ralchenko, A. V. Khomich and R. A. Khemelnitskiy, *Electrochim. Acta*, 2003, **49**, 41–49.
33 Y. V. Pleskov, M. D. Krotova, V. V. Elkin, V. G. Ralchenko, A. V. Khomich and R. A. Khmelnitskiy, *Electrochim. Acta*, 2005, **50**, 1149–1156.
34 F. Maier, M. Riedel, B. Mantel, J. Ristein and L. Ley, *Phys. Rev. Lett.*, 2000, **85**, 3472–3475.
35 J. Ristein, M. Riedel and L. Ley, *J. Electrochem. Soc.*, 2004, **151**, E315–E325.
36 J. Ristein, *Appl. Phys. A: Mater. Sci. Process.*, 2006, **82**(3), 377–384.
37 V. Chakrapani, S. C. Eaton, A. B. Anderson, M. Tabib-Azar and J. C. Angus, *Electrochem. Solid-State Lett.*, 2005, **8**, E4–E8.
38 I. M. Landstrass and K. V. Ravi, *Appl. Phys. Lett.*, 1989, **55**, 975–977.
39 C. E. Nebel, in *Thin-Film Diamond I, Semiconductors and Semimetals*, ed. C. E. Nebel and J. Ristein, Elsevier, Amsterdam, 2003, vol. 76, p. 261.
40 C. E. Nebel, *Semicond. Sci. Technol.*, 2003, **18**(3), S1–S11.
41 M. Nesladek, K. Haenen and M. Vanecek, in *Thin-Film Diamond I, Semiconductors and Semimetals*, ed. C. E. Nebel and J. Ristein, Elsevier, Amsterdam, 2003, vol. 76, p. 325.
42 J. A. Carlisle and O. Auciello, *Interface*, 2003, **12**(1), 28–31.
43 C. E. Nebel, D. Shin, B. Rezek, N. Tokuda, H. Uetsuka and H. Watanabe, *J. R. Soc. Interface*, 2007, **4**, 439–461.
44 E. Mahe, D. Devilliers and Ch. Comninellis, *Electrochim. Acta*, 2005, **50**, 2263–2277.
45 O. Enea, B. Riedo and G. Dietler, *Nano Lett.*, 2002, **2**(3), 241–244.
46 P. Bou and L. Vandenbulcke, *J. Electrochem. Soc.*, 1991, **138**(10), 2991–3000.
47 Y. Wang, D. C. Alsmeyer and R. L. McCreery, *Chem. Mater.*, 1990, **2**, 557–563.
48 Y. V. von Kaenel and J. S. E. Blank, *Diamond Relat. Mater.*, 1995, **4**, 972–976.

49 V. Palshin, E. I. Meletis, S. Ves and S. Logothetidis, *Thin Solid Films*, 1995, **270**, 165–172.
50 T. N. Rao, D. A. Tryk, K. Hashimoto and A. Fujishima, *J. Electrochem. Soc.*, 1999, **146**, 680–684.
51 K. Kinoshita, *Carbon: Electrochemical and Physicochemical Properties*, John Wiley and Sons, New York, 1988.
52 H. Notsu, I. Yagi, T. Tatsuma, D. A. Tryk and A. Fujishima, *J. Electroanal. Chem.*, 2000, **492**, 31–37.
53 H. Notsu, T. Fukazawa, T. Tatsuma, D. A. Tryk and A. Fujishima, *Electrochem. Solid-State Lett.*, 2001, **4**, H1–H3.
54 H. Masuda, M. Watanabe, K. Yasui, D. A. Tryk, T. N. Rao and A. Fujishima, *Adv. Mater.*, 2000, **12**, 444–447.
55 G. Siné, L. Ouattara, M. Panizza and Ch. Comninellis, *Electrochem. Solid-State Lett.*, 2003, **6**, D9–D11.
56 S. Ferro and A. De Battisti, *J. Phys. Chem. B - Condensed Phase*, 2003, **8**(7), 7567–7573.
57 P. Bouvier, D. Delabouglise, A. Denoyelle, B. Marcus, M. Mermoux and J.-P. Petit, *Electrochem. Solid-State Lett.*, 2005, **8**, E57–E61.
58 T. Kondo, K. Honda, D. A. Tryk and A. Fujishima, *J. Electrochem. Soc.*, 2005, **152**, E18–E23.
59 A. Sarapuu, K. Helstein, D. J. Schiffrin and K. Tammeveski, *Electrochem. Solid-State Lett.*, 2005, **8**, E30–E33.
60 D. Shin, N. Tokuda, B. Rezek and C. E. Nebel, *Electrochem. Commun.*, 2006, **8**, 844–850.
61 T. Matrab, M. M. Chehimi, J. P. Boudou, F. Benedic, J. Wang, N. N. Naguib and J. A. Carlisle, *Diamond Relat. Mater.*, 2006, **15**, 639–644.
62 P. Krysiński, Y. Show, J. Stotter and G. J. Blanchard, *J. Am. Chem. Soc.*, 2003, **125**(42), 12726–12728.
63 M. Hyde, A. J. Saderlay, S. J. Wilkins, J. S. Foord, R. G. Compton and F. Marken, *J. Solid State Electrochem.*, 2002, **6**, 183–187.
64 N. Spãtaru, C. Terashima, K. Tokuhiro, I. Sutanto, D. A. Tryk, S.-M. Park and A. Fujishima, *J. Electrochem. Soc.*, 2003, **150**, E337–E341.
65 A. Chatterjee and J. Foord, *Diamond Relat. Mater.*, 2006, **15**, 664–667.
66 A. Manivannan, N. Spãtaru, K. Arihara and A. Fujishima, *Electrochem. Solid-State Lett.*, 2005, **8**, C138–C140.
67 M. J. Bonne, M. Helton, K. Edler and F. Marken, *Electrochem. Commun.*, 2007, **9**, 42–48.
68 F. Shang, Y. Liu, S. Hrapovic, J. D. Glennon and J. H. T. Luong, *Analyst*, 2009, **134**, 519–527.
69 F. Shang, L. Zhou, K. A. Mahmoud, S. Hrapovic, Y. Liu, H. A. Moynihan, J. D. Glennon and J. H. T. Luong, *Anal. Chem.*, 2009, **81**(10), 4089–4098.
70 F. Shang, J. D. Glennon and J. H. T. Luong, *J. Phys. Chem. C*, 2008, **112**, 20258–20263.
71 T. A. Ivandini, R. Sato, Y. Makide, A. Fujishima and Y. Einaga, *Diamond Relat. Mater.*, 2004, **13**, 2003–2008.
72 T. A. Ivandini, R. Sato, Y. Makide, A. Fujishima and Y. Einaga, *Diamond Relat. Mater.*, 2005, **14**, 2133–2138.
73 T. A. Ivandini, R. Sato, Y. Makide, A. Fujishima and Y. Einaga, *Anal. Chem.*, 2006, **78**, 6291–6298.
74 G. Siné, I. Duo, B. El Roustom, G. Foti and Ch. Comninellis, *J. Appl. Electrochem.*, 2006, **36**, 847–862.
75 I. Duo, P.-A. Michaud, W. Haenni, A. Perret and Ch. Comninellis, *Electrochem. Solid-State Lett.*, 2000, **3**, 325–326.
76 K. J. McKenzie and F. Marken, *Electrochem. Solid-State Lett.*, 2002, **5**, E47–E50.
77 J. A. Bennett, Y. Show, S. Wang and G. M. Swain, *J. Electrochem. Soc.*, 2005, **152**, E184–E192.
78 G. Siné, G. Foti and Ch. Comninellis, *J. Electroanal. Chem.*, 2006, **595**, 115–124.
79 C. M. Welch, A. O. Simm and R. G. Compton, *Electroanalysis*, 2006, **18**(10), 965–970.
80 A. O. Simm, X. Ji, C. E. Banks, M. E. Hyde and R. G. Compton, *ChemPhysChem*, 2006, **7**(3), 704–709.
81 L. Tang, C. Tsai, W. W. Gerberich, L. Kruckeberg and D. R. Kania, *Biomaterials*, 1995, **16**(6), 483–488.
82 H. J. Mathieu, *Surf. Interface Anal.*, 2001, **32**, 3–9.
83 F. Z. Cui and D. J. Li, *Surf. Coat. Technol.*, 2000, **131**, 481–487.
84 K. Takahashi, M. Tanga, O. Takai and H. Okamura, *BioIndustry*, 2000, **17**(6), 44–51.
85 K. Takahashi, M. Tanga, O. Takai and H. Okamura, *Diamond Relat. Mater.*, 2003, **12**(3–7), 572–576.
86 J. Wang, M. A. Firestone, O. Auciello and J. A. Carlisle, *Langmuir*, 2004, **20**(26), 11450–11456.
87 G.-J. Zhang, K. S. Song, Y. Nakamura, T. Ueno, T. Funatsu, I. Ohdomari and H. Kawarada, *Langmuir*, 2006, **22**(8), 3728–2734.
88 W. Yang, O. Auciello, J. E. Butler, W. Cai, J. A. Carlisle, J. E. Gerbi, D. M. Gruen, T. Knickerbocker, T. L. Lasseter, J. N. Russell Jr, L. M. Smith and R. J. Hamers, *Nat. Mater.*, 2002, **1**, 253–257.
89 S. Ferro and A. De Battisti, *Anal. Chem.*, 2003, **75**, 7040–7042.
90 S. Wang and G. M. Swain, *J. Phys. Chem. C*, 2007, **111**, 3986–3995.
91 N. R. Wilson, S. L. Clewes, M. E. Newton, P. R. Unwin and J. V. Macpherson, *J. Phys. Chem. B*, 2006, **110**, 5639–5646.
92 R. L. McCreery, *Chem. Rev.*, 2008, **108**, 2646–2687.
93 M. C. Granger, M. Witek, J. Xu, J. Wang, M. Hupert, A. Hanks, M. D. Koppang, J. E. Butler, G. Lucazeau, M. Mermoux, J. W. Strojek and G. M. Swain, *Anal. Chem.*, 2000, **72**, 3793–3804.
94 S. Ranganathan, T.-C. Kuo and R. L. McCreery, *Anal. Chem.*, 1999, **71**, 3574–3580.
95 Y. Pleskov, M. Krotova, V. Ralchenko, A. Saveliev and A. Bozhko, *Russ. J. Electrochem.*, 2007, **43**, 827–836.
96 A. Kraft, *Int. J. Electrochem. Sci.*, 2007, **2**, 355–385.
97 L. L. G. Silva, N. G. Ferreira, M. Dotto and M. U. Kleinke, *Appl. Surf. Sci.*, 2001, **181**(3–4), 327–330.
98 M. Yoshimura, K. Honda, R. Uchikado, T. Kondo, T. N. Rao, D. A. Tryk, A. Fujishima, Y. Sakamoto, K. Yasui and H. Masuda, *Diamond Relat. Mater.*, 2001, **10**, 620–626.
99 M. Yoshimura, K. Honda, T. Kondo, R. Uchikado, Y. Einaga, T. N. Rao, D. A. Tryk and A. Fujishima, *Diamond Relat. Mater.*, 2002, **11**, 67–74.
100 G. Pastor-Moreno and D. J. Riley, *Electrochim. Acta*, 2002, **47**, 2589–2595.
101 E. Fortin, E. Vieil, P. Mailley, S. Szunerits and T. Livache, *Anal. Chem.*, 2007, **79**(10), 3741–3746.
102 I. L. Codognoto, S. A. S. Machado and L. A. Avaca, *J. Appl. Electrochem.*, 2003, **33**, 951–957.
103 J. Xu and G. M. Swain, *Anal. Chem.*, 1998, **70**, 1502–1510.
104 M. C. Granger, J. Xu, J. W. Strojek and G. M. Swain, *Anal. Chim. Acta*, 1999, **397**, 145–161.
105 A. Suzuki, T. A. Ivandini, A. Kamiya, S. Nomura, M. Yamanuki, K. Matsumoto, A. Fujishima and Y. Einaga, *Sens. Actuators, B*, 2007, **120**, 500–507.
106 C. Batchelor-McAuley, C. E. Banks, A. O. Simm, T. G. J. Jones and R. G. Compton, *Analyst*, 2006, **131**, 106–110.
107 O. Chailapakul, M. Amatatongchai, P. Wilairat, K. Grudpan and D. Nacapricha, *Talanta*, 2004, **64**, 1253–1258.
108 C. M. Welch, M. E. Hyde, C. E. Banks and R. G. Compton, *Anal. Sci.*, 2005, **21**, 1421–1430.
109 T. Ochiai, K. Arihara, C. Terashima and A. Fujishima, *Chem. Lett.*, 2006, **35**, 1018–1019.
110 C. Provent, W. Haenni, E. Santoli and P. Rychen, *Electrochim. Acta*, 2004, **49**, 3737–3744.
111 N. S. Lawrence, M. Pagels, A. Meredith, T. G. J. Jones, C. E. Hall, C. S. J. Pickles, H. P. Godfried, C. E. Banks, R. G. Compton and L. Jiang, *Talanta*, 2006, **69**, 829–834.
112 A. Chatterjee, R. Wiltshire, K. B. Holt, R. G. Compton, J. S. Foord and F. Marken, *Diamond Relat. Mater.*, 2002, **11**, 646–650.
113 P. Sonthalia, E. McGaw, Y. Show and G. M. Swain, *Anal. Chim. Acta*, 2004, **522**(1), 35–44.
114 J. S. Foord, K. Eaton, W. Hao and A. Crossley, *Phys. Chem. Chem. Phys.*, 2005, **7**, 2787–2792.
115 E. A. McGaw and G. M. Swain, *Anal. Chim. Acta*, 2006, **575**(2), 180–189.
116 I. Tröster, L. Schäfer, M. Fryda and T. Matthee, *Water Sci. Technol.*, 2004, **49**(4), 207–212.
117 S. Hrapovic, Y. Liu and J. H. T. Luong, *Anal. Chem.*, 2007, **79**, 500–507.
118 C. E. Banks, M. E. Hyde, P. Tomcik, R. Jacobs and R. G. Compton, *Talanta*, 2004, **62**, 279–286.
119 C. Prado, S. J. Wilkins, F. Marken and R. G. Compton, *Electroanalysis*, 2002, **14**, 262–272.
120 A. Manivannan, L. Ramakrishnan, M. S. Seehra, E. Granite, J. E. Butler, D. A. Tryk and A. Fujishima, *J. Electroanal. Chem.*, 2005, **577**, 287–293.
121 A. Manivannan, M. S. Seehra and A. Fujishima, *Fuel Process. Technol.*, 2004, **85**, 513–519.

122 A. J. Saterlay, J. S. Foord and R. G. Compton, *Analyst*, 1999, **124**, 1791–1796.
123 Y. Zhang and S. Yoshihara, *J. Electroanal. Chem.*, 2004, **573**, 327–331.
124 A. J. Saterlay, D. F. Tibbetts and R. G. Compton, *Anal. Sci.*, 2000, **16**, 1055–1060.
125 C. Prado, S. J. Wilkins, P. Gründler, F. Marken and R. G. Compton, *Electroanalysis*, 2003, **15**, 1011–1016.
126 S. Xie, G. Shafer, C. G. Wilson and H. B. Martin, *Diamond Relat. Mater.*, 2006, **15**, 225–228.
127 N. Spătaru, B. V. Sarada, D. A. Tryk and A. Fujishima, *Electroanalysis*, 2002, **14**, 721–728.
128 T. N. Rao, B. H. Loo, B. V. Sarada, C. Terashima and A. Fujishima, *Anal. Chem.*, 2002, **74**, 1578–1583.
129 O. Chailapakul, A. Fujishima, P. Tipthara and H. Siriwongchai, *Anal. Sci.*, 2001, **17**(Suppl), i419–i422.
130 A. Fujishima and T. N. Rao, *Diamond Relat. Mater.*, 2001, **10**, 1799–1803.
131 L. Codognoto, S. A. S. Machado and L. A. Avaca, *Diamond Relat. Mater.*, 2002, **11**, 1670–1675.
132 Y. L. Zhou and J. F. Zhi, *Electrochem. Commun.*, 2006, **8**, 1811–1816.
133 N. Spătaru, B. V. Sarada, E. Popa, D. A. Tryk and A. Fujishima, *Anal. Chem.*, 2001, **73**, 514–519.
134 A. Fujishima, T. N. Rao, E. Popa, B. V. Sarada, I. Yagi and D. A. Tryk, *J. Electroanal. Chem.*, 1999, **473**, 179–185.
135 C. C. Chang, L. C. Chen, S. J. Liu and H. C. Chang, *Anal. Lett.*, 2006, **39**, 2581–2589.
136 K. Ohnishi, Y. Einaga, H. Notsu, C. Terashima, T. N. Rao, S.-G. Park and A. Fujishima, *Electrochem. Solid-State Lett.*, 2002, **5**, D1–D3.
137 T. N. Rao, T. A. Ivandini, C. Terashima, B. V. Sarada and A. Fujishima, *New Diamond Front. Carbon Technol.*, 2003, **13**(2), 79–108.
138 B. V. Sarada, T. N. Rao, D. A. Tryk and A. Fujishima, *Anal. Chem.*, 2000, **72**, 1632–1638.
139 V. A. Pedrosa, L. Codognoto, S. A. S. Machado and L. A. Avaca, *J. Electroanal. Chem.*, 2004, **573**, 11–18.
140 C. Prado, G.-U. Flechsig, P. Gründler, J. S. Foord, F. Marken and R. G. Compton, *Analyst*, 2002, **127**(3), 329–333.
141 T. A. Ivandini, T. N. Rao, A. Fujishima and Y. Einaga, *Anal. Chem.*, 2006, **78**, 3467–3471.
142 N. Wangfuengkanagul and O. Chailapakul, *Talanta*, 2002, **58**, 1213–1219.
143 M. D. Koppang, M. Witek, J. Blau and G. M. Swain, *Anal. Chem.*, 1999, **71**, 1188–1195.
144 M. A. Witek and G. M. Swain, *Anal. Chim. Acta*, 2001, **440**, 119–129.
145 T. A. Ivandini, K. Honda, T. N. Rao, A. Fujishima and Y. Einaga, *Talanta*, 2007, **71**, 648–655.
146 J. M. Halpern, S. Xie, G. P. Sutton, B. T. Higashikubo, C. A. Chestek, H. Lu, H. J. Chiel and H. B. Martin, *Diamond Relat. Mater.*, 2006, **15**, 183–187.
147 T. N. Rao, B. V. Sarada, D. A. Tryk and A. Fujishima, *J. Electroanal. Chem.*, 2000, **491**, 175–181.
148 N. Wangfuengkanagul, W. Siangproh and O. Chailapakul, *Talanta*, 2004, **64**, 1183–1188.
149 W. Siangproh, N. Wangfuengkanagul and O. Chailapakul, *Anal. Chim. Acta*, 2003, **499**(1–2), 183–189.
150 S. Jolley, M. Koppang, T. Jackson and G. M. Swain, *Anal. Chem.*, 1997, **69**, 4099–4107.
151 P. Bouvrette, S. Hrapovic, K. B. Male and J. H. T. Luong, *J. Chromatogr., A*, 2006, **1103**(2), 248–256.
152 A. Preechaworapun, S. Chuanuwatanakul, Y. Einaga, K. Grudpan, S. Motomizu and O. Chailapakul, *Talanta*, 2006, **68**, 1726–1731.
153 C. Terashima, T. N. Rao, B. V. Sarada and A. Fujishima, *Chem. Lett.*, 2003, **32**, 136–137.
154 O. Chailapakul, W. Siangproh, B. V. Sarada, C. Terashima, T. N. Rao, D. A. Tryk and A. Fujishima, *Analyst*, 2002, **127**, 1164–1168.
155 J. Wang, G. Chen, A. Muck, Jr, D.-C. Shin and A. Fujishima, *J. Chromatogr., A*, 2004, **1022**, 207–212.
156 J. Wang, G. Chen, M. P. Chatrathi, A. Fujishima, D. A. Tryk and D.-C. Shin, *Anal. Chem.*, 2003, **75**(4), 935–939.
157 K. Stolarczyk, E. Nazaruk, J. Rogalski and R. Bilewicz, *Electrochem. Commun.*, 2007, **9**, 115–118.
158 A. Härtl, E. Schmich, J. A. Garrido, J. Hernando, S. R. Catharino, S. Walter, P. Feulner, A. Kromka, D. Steinmüller and M. Stutzmann, *Nat. Mater.*, 2004, **3**, 736–742.
159 W. Yang, J. E. Butler, J. N. Russell and R. J. Hamers, *Langmuir*, 2004, **20**, 6778–6784.
160 C. McClintock, V. Kertesz and R. L. Hettich, *Anal. Chem.*, 2008, **80**(9), 3304–331.
161 S. Hasoň, H. Pivokov, V. Vetterl and M. Fojta, *Anal. Chem.*, 2008, **80**(7), 2391–2399.
162 A. Suzuki, T. A. Ivandini, K. Yoshimi, A. Fujishima, G. Oyama, T. Nakazato, N. Hattori, S. Kitazawa and Y. Einaga, *Anal. Chem.*, 2007, **79**(22), 8608–8615.
163 A. Preechaworapun, T. A. Ivandini, A. Suzuki, A. Fujishima, O. Chailapakul and Y. Einaga, *Anal. Chem.*, 2008, **80**(6), 2077–2083.
164 M. Chiku, J. Nakamura, A. Fujishima and Y. Einaga, *Anal. Chem.*, 2008, **80**(15), 5783–5787.
165 J. Weng, J. Zhang, H. Li, L. Sun, C. Lin and Q. Zhang, *Anal. Chem.*, 2008, **80**(18), 7075–7083.
166 E. Bitziou, D. O'Hare and B. A. Patel, *Anal. Chem.*, 2008, **80**(22), 8733–8740.
167 T. N. Rao, I. Yagi, T. Miwa, D. A. Tryk and A. Fujishima, *Anal. Chem.*, 1999, **71**(13), 2506–2511.
168 E. Majid, K. B. Male and J. H. T. Luong, *J. Agric. Food Chem.*, 2008, **56**(17), 7691–7695.
169 K. B. Holt, J. Hu and J. S. Foord, *Anal. Chem.*, 2007, **79**(6), 2556–2561.
170 M. Wei, C. Terashima, M. Lv, A. Fujishima and Z.-Z. Gu, *Chem. Commun.*, 2009, 3624–3626.
171 J. Rubio-Retama, J. Hernando, B. López-Ruiz, A. Härtl, D. Steinmüller, M. Stutzmann, E. López- Cabarcos and J. A. Garrido, *Langmuir*, 2006, **22**(13), 5837–5842.
172 J. Wu and Y. Qu, *Anal. Bioanal. Chem.*, 2006, **385**(7), 1330–1335.
173 S. Hrapovic, Y. Liu, K. B. Male and J. H. T. Luong, *Anal. Chem.*, 2004, **76**(4), 1083–1088.
174 M. Pagels, C. E. Hall, N. S. Lawrence, A. Meredith, T. G. J. Jones, H. P. Godfried, C. S. J. Pickles, J. Wilman, C. E. Banks, R. G. Compton and L. Jiang, *Anal. Chem.*, 2005, **77**(11), 3705–3708.
175 A. L. Colley, C. G. Williams, U. D'Haenens-Johansson, M. E. Newton, P. R. Unwin, N. R. Wilson and J. V. Macpherson, *Anal. Chem.*, 2006, **78**(8), 2539–2548.
176 J. Jia, D. Kato, R. Kurita, Y. Sato, K. Maruyama, K. Suzuki, S. Hirono, T. Ando and O. Niwa, *Anal. Chem.*, 2007, **79**(1), 98–105.
177 http://www.biosciencetechnology.com.
178 D. Plumlee, P. D. Mudget and J. R. Shultz, SAE Technical Paper, 2002, doc. no. 2002-01-2537.